AN INEXPENSIVE AERIAL PLATFORM FOR PRECISE REMOTE SENSING OF ALMOND AND WALNUT CANOPY TEMPERATURE

K. Crawford, J. Roach, R. Dhillon, F. Rojo, S. Upadhyaya

Biological Systems Engineering Department
University of California, Davis
Davis, California

ABSTRACT

Monitoring water stress in specialty crops to increase water use efficiency (WUE) is becoming more necessary when faced with the reality of depleting water resources. Leaf temperature (T_L) of almond [*prunus dulcis*] and walnut [*juglans regia*] trees has been shown to be closely linked to stem water potential, a sensitive indicator of stress in woody plants.

This study was conducted to explore the feasibility of remotely measuring canopy temperature (T_{can}) of walnut and almond trees with a small, inexpensive unmanned aerial vehicle (UAV). An infrared (IR) point sensor was installed with a lightweight camera on the underside of a multi-rotor UAV. The UAV was flown over a targeted tree canopy recording temperature and images. Image classification was used to identify the ground contents of each temperature measurement, and a linear system of equations utilizing the image/temperature records pertaining to a targeted tree canopy was established to approximate the temperature of the sunlit and shaded portions of that canopy.

Analyses of three flights over almond tree canopies approximated the temperatures of the sunlit and shaded portions of the canopies within an average of 2.2^{o}C of their respective ground truths for both portions, and analyses of four flights over walnut canopies approximated the sunlit and shaded portions within 1.0 and 1.3^{o}C of their respective ground truths, the average difference for all temperature approximations between the seven trees being 1.5^{o}C. With canopy temperatures ranging from 16 to 40°C, the approximations fit a linear trend with a coefficient of determination (r^2 value) of 0.96.

The use of an IR sensor coupled with a camera to establish a linear system of equations for individual trees showed promising ability to approximate a tree's canopy temperature. This method also has the advantage of distinguishing between the sunlit and shaded portions of the canopy.

Keywords: precision agriculture, remote sensing, UAV, infrared

INTRODUCTION

Irrigation water is becoming a scarcer and more valuable resource as a result of fluctuating rain patterns, depleting ground water resources, and fierce competition from a growing urban population. An inexpensive method to monitor a crop's precise irrigation needs that can cover a large area with high temporal and spatial resolution could help improve the efficiency with which those resources are used.

Carruthers et al. (1997) distinguished two types of water use efficiency (WUE): paper and real WUE. Paper WUE sees evaporation, runoff, and deep percolation as sources of inefficiency, while real WUE looks instead at the final use of the water before it enters an unusable state. The water is considered unusable after it is evaporated, is heavily polluted, is consumed in a product, or flows to an unreachable location. Real WUE ignores runoff and seepage losses, because those resources are typically reused further down in a watershed. In agriculture, the real WUE model, also referred to as water productivity (WP), looks at the amount of yield produced by the crop (or plant) per unit of evapotranspiration (ET). Yield on its own, however, is not the only measure of productivity in most crops. Much of the value in specialty crops is determined by the quality of the yield, and this should also be considered in the determination of WP (Kijne et al., 2003).

Regulated deficit irrigation (RDI) aims to improve WP by inducing certain levels of stress at appropriate stages of plant growth by watering below ET demands. Though reducing ET does reduce overall biomass growth, it does not necessarily reduce yield due to physiological changes induced in the plant. RDI in California olives was able to save 25% of irrigation water with little to no impact on yield (Goldhamer, 1999). Studies of other woody species have shown similarly improved WP with varying levels of RDI with little to no effect on yield (Fereres and Soriano, 2007; Intrigliolo and Castel, 2010), and even increases in yield and/or quality (Chaves et al., 2010; Cui et al., 2008).

Stem water potential (ψ_{stem}) has been closely linked to stomatal regulation (Naor, 1998), a plant's primary means of regulating its water usage, and it has been shown to be a robust method to monitor plant water status in grapes and woody tree species (Garnier and Berger, 1985; Jensen et al., 1990; McCutchan and Shackel, 1992; Shackel, 2011). The Scholander pressure chamber has been the gold standard to measure ψ_{stem} for several decades (Scholander et al., 1965), but it is too bulky and cumbersome for use in monitoring large fields.

Udompetaikul (2012) developed a sensor suite to detect ψ_{stem} in almonds and walnuts through T_L. He was able to show that an average shaded T_L, when adjusted for wind speed, relative humidity, and incident sunlight, was related to ψ_{stem} in almonds and walnuts. Although this mobile sensor suite had the advantage of monitoring SWP proximally and was faster to use than the Scholander pressure chamber, it still required walking or driving through the field and stopping to make hand measurements of 5-10 leaves on a given plant.

In unpublished work at the University of California, Davis, a more convenient handheld sensor suite (HHSS) was developed to measure the same variables. Though this HHSS was much smaller and faster to use than the Scholander pressure chamber and the sensor suite developed by Udompetaikul (2012), it did

not reduce the time required to travel through the field or the amount of measurements needed for each plant.

With a faster method to measure T_L, the environmental variables could be obtained using a weather station or similar method to greatly increase the speed with which plants are monitored. Satellite and aerial platforms with thermal infrared (IR) imagers can cover huge swaths of land, but they have serious limitations when used in precision agriculture applications (Moran et al., 1997; Mulla, 2013). Satellites are very expensive to launch and operate, they typically do not have high enough spatial resolution for precision applications, do not provide frequent enough coverage, and the data they provide is not readily accessible to the average user (Anderson et al., 2012; Mulla, 2013; Seelan et al., 2003).

Unmanned aerial vehicles (UAV) have shown potential to replace satellite or aerial imagery in precision applications (Xiang and Tian, 2011). UAVs are relatively low-cost, easily and quickly deployable, fly at low altitudes and slow speeds to allow for very high resolution, and are highly adaptable to customized applications. UAVs also have the advantage of being a very hands-on, approachable platform, which could potentially help bridge the gap between the information available from remote sensing and potential user. Such systems have already been tested in orchard crops and vineyards (Baluja et al., 2012; Gonzalez-Dugo et al., 2013) using thermal cameras.

The feasibility of using such a platform is apparent, but the thermal imagers typically employed on these platforms do not have adequate accuracy in measured temperature to estimate ψ_{stem}, and are fairly expensive. The system employed by Gonzalez-Dugo et al. (2013), for example, is advertised to be accurate to within $2^{o}C$, and it still does not provide the spatial resolution necessary to identify temperature gradients within a given canopy. This ability is important, because a typical canopy is composed of both shaded and sunlit portions, which can routinely have substantial differences in temperature of $5\text{-}10^{o}C$. These systems are more useful for showing relative differences in vegetative health throughout a field. In order to get a more precise reading on T_L, and subsequently on ψ_{stem}, a sensor with greater accuracy is required. Inexpensive point sensors can typically provide accuracies of up to $0.5^{o}C$, and would be of greater use in precise monitoring of ψ_{stem}.

The objective of this study was to explore the feasibility of using an inexpensive IR sensor on a small UAV to reliably measure T_L of almond and walnut trees in Northern California.

MATERIALS & METHODS

IR sensor

A Melexis (Melexis Microelectronic Systems; Rozendaalstraat 12 Ieper, Belgium) MLX90614xCF IR point sensor was used for measuring T_L. The sensor has a barrel-type covering which limits the direction from which thermal radiation contacts the thermopile. That barrel creates an angular field of view (FOV) within which the sensor detects radiation. This particular sensor's FOV covered a circular area of about 20° in angular width. In order to further narrow the FOV, a

parabolic mirror was employed which theoretically would narrow the FOV of the IR sensor to parallel rays, or zero degrees.

Before putting the sensor to use, the sensor's actual FOV was determined by fixing the sensor in front of an ice bath with a wooden board between them. The board was incrementally moved to the side, slowly exposing the much colder ice bath behind it. The point along the horizontal axis (indicated by the edge of the board) at which the measured temperature began to transition from the temperature of the board to the temperature of the ice bath indicated the effective edge of the FOV. The edges in both the x and y axes were established in this manner. The final FOV ended up being about 13° in width.

The width of the FOV of this sensor dictated the allowable flight altitude in order for the ground track of the IR sensor to be no bigger than the tree canopy. With a FOV of 13° and assuming a tree canopy of 30 feet in diameter, the IR sensor would need to be less than 132 feet above the tree canopy if perfectly centered. Realistically, the UAV would not be perfectly centered above each canopy, so flights were conducted at a more conservative altitude between 50 and 75 feet.

Camera platform

A Tetracam (Tetracam, Inc. 21601 Devonshire St. Chatsworth, CA) ADC Lite was used to provide spatial awareness for the temperature measurements. This camera captures images in red, green, and near-infrared (NIR) bands, and is widely sued in agricultural applications. A custom gimbal was fabricated to attach the camera and IR sensor to the UAV. The gimbal had two degrees of rotation to compensate for roll and yaw by the UAV. An inertial measurement unit measured acceleration and rotation rate in both axes for use in a feedback loop to control two DC brushless motors on each axis. This control system allowed the frame, with the camera mounted on it, to compensate for the unpredictable attitude changes of the UAV in order to keep the camera pointed straight down at the targeted canopy. The bracket designed for the IR sensor and parabolic mirror was hard-mounted with the camera, allowing the camera FOV and the IR FOV to be fixed together. This frame attached to the underside of the UAV.

Methodology

The installation of the camera and IR sensor allowed for the FOV of the IR sensor to be defined with respect to the camera FOV. The approximate FOV of the IR sensor is shown in Fig. 1, traced in a typical image captured by the setup.

Fig. 1. The yellow circle illustrates the IR sensor FOV as seen in a typical image of a walnut canopy. The checkered targets were used for GPS reference.

Relating the IR sensor's FOV to the camera's FOV gave us a spatial awareness of where the IR sensor was pointing, as well as detailed information of what it was pointing at. Through the use of a small control board, the camera and the IR sensor were timed such that each image had an accompanying IR temperature measurement, as well as a GPS tag from the UAV autopilot. The image could then be used to determine the contents of the target of the IR temperature sensor, based on the pixels contained within the FOV circled in Fig. 1. The target was assumed to consist of four distinct classes of material: sunlit leaves, shaded leaves, sunlit soil, and shaded soil. These four classes represented the material in the vast majority of pixels in each image, with each class assumed to have a fairly uniform, distinct temperature. Instead of trying to solve for the temperature of individual leaves, we looked at the average temperature of all sunlit leaves, and the average temperature of all shaded leaves. Accordingly, these temperatures will be referred to as T_{can}, instead of T_L. The soil, of course, was not a desired target, but it could not be ignored in cases of less than 100% canopy cover, as it appeared through gaps in the canopy and around the edges of the canopy.

Fig. 2 is a typical image of a walnut canopy during one of the trials. In order to illustrate classification of the hundreds of thousands of pixels in the FOV of the IR sensor, a sampling of pixels, identified by the scatter of colored dots, known to be of each class of material is identified in the image. The colors correspond to pixels considered to be of the same class. Pixels were chosen with the attempt to represent the range of each class in terms of its appearance in the image. To illustrate the classification process, the 8-bit values of those pixels in the NIR versus green bands are plotted in Fig. 3.

The yellow dots in Fig. 3 are a random sampling of the image, illustrating the range of values seen in any particular pixel. Intuitively, each class occupies its own region in this two-dimensional space. In order to differentiate between the four classes, we first defined boundaries between the pixels of vegetation and soil and between the sunlit and shaded pixels using a discriminant analysis method. Those two boundaries were then used to determine the class of any given pixel based on its location in this two-dimensional space.

Fig. 2. The pixels identified by colored dots were determined to be representative of each class of material: sunlit leaves, shaded leaves, sunlit soil, and shaded soil.
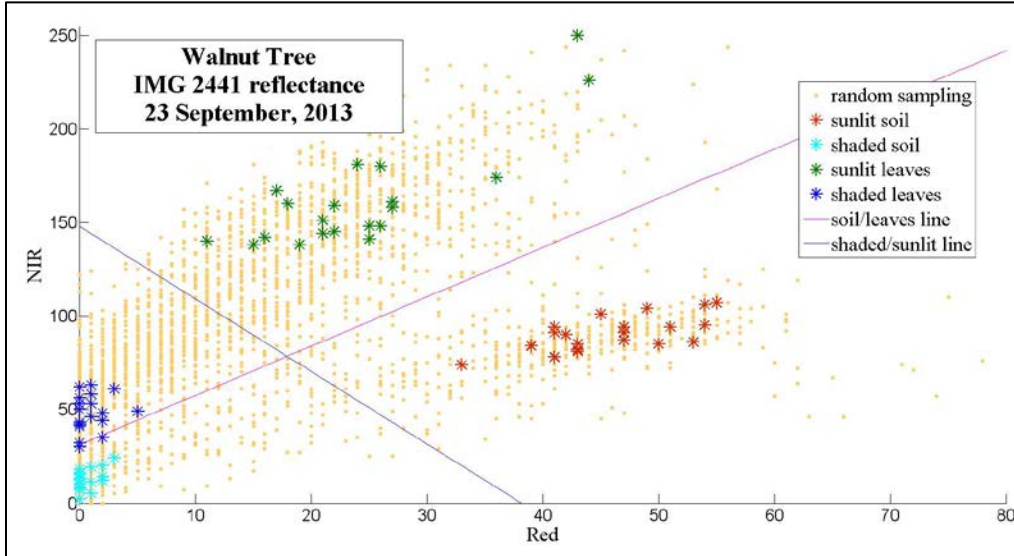

Fig. 3. The 8-bit NIR and red values of the pixels identified in Fig. 2 are plotted to illustrate the classification process.

Each temperature measurement was assumed to be a weighted sum of the temperatures of these four classes of material. The weight assigned to the temperature contribution for each class in equation (1) was determined by the physical area (A_i) it covered in the IR sensor's FOV.

$$T_{meas} = \frac{T_a A_a + T_b A_b + T_c A_c + T_d A_d}{A_a + A_b + A_c + A_d} \quad (1)$$

In equation (1), T_a, T_b, T_c, and T_d represent the average temperature of each class (unknowns), T_{meas} represents the temperature measured by the airborne IR sensor, and A_a, A_b, A_c, and A_d represent the respective areas each class occupied

in the FOV of the IR sensor. The A_i terms simplify to be a count of the pixels of each class resulting from the classification process.

Each image/temperature record provided T_{meas}, A_a, A_b, A_c, and A_d in equation (1), leaving T_a, T_b, T_c, and T_d unknown. With at least four records of the same target, a linear set of equations could be established to solve for T_a, T_b, T_c, and T_d. The T_{meas} from the IR sensor and the A_i terms from the classification results were used to establish a linear system of equations of the form:

$$Ax = b \tag{2}$$

where the A matrix represents the A_i terms of equation (1), the x vector represents the unknown T_i terms on the right-hand side of equation (1), and the b vector represents T_{meas}. An example system, composed of n measurements of the same target canopy, is represented in equation (3):

$$\begin{bmatrix} A_{1a} & A_{1b} & A_{1c} & A_{1d} \\ A_{2a} & A_{2b} & A_{2c} & A_{2d} \\ A_{3a} & A_{3b} & A_{3c} & A_{3d} \\ A_{4a} & A_{4b} & A_{4c} & A_{4d} \\ & & \vdots & \\ A_{na} & A_{nb} & A_{nc} & A_{nd} \end{bmatrix} \begin{bmatrix} T_a \\ T_b \\ T_c \\ T_d \end{bmatrix} = \begin{bmatrix} T_1 \\ T_2 \\ T_3 \\ T_4 \\ \vdots \\ T_n \end{bmatrix} + \begin{bmatrix} e_1 \\ e_2 \\ e_3 \\ e_4 \\ \vdots \\ e_n \end{bmatrix} \tag{3}$$

where T_1 … T_n represent each measured temperature of the same target canopy, and each row of the A and b matrices represents one image/temperature record. There is also an error associated with each record to account for classification errors, sampling errors, electronic noise, environmental variables, and any other unforeseen and uncontrollable variables. The system was approximated using QR decomposition, which applies a linear least-squares fit to the data represented by the system of equations. In practice, the more image/temperature records obtained of the target, the better T_a, T_b, T_c, and T_d can be approximated. In this study, we strove to produce as many records as possible for each set of equations, typically ranging between 10 and 30 records.

Data collection

Nine flights were performed in September of 2013 between almond and walnut orchards. The orchards were owned by the University of California, Davis, at the Nickels Soil Management Laboratory near Arbuckle, CA. Flights were typically conducted around solar noon in sunny, calm conditions, with the exception of the two flights done on 28 September, which were conducted in early morning under lower light conditions. These flights were performed to explore the robustness of T_{can} measurements under varying light and temperature conditions.

Immediately before each flight, ground temperature measurements of each class in the target area were taken using the HHSS mentioned previously. Twenty temperature measurements were taken each of sunlit and shaded leaves of the target canopy, split between the bottom of the tree and the top of the tree, as well as ten measurements each of sunlit and shaded soil right around the tree. The

temperature samples of each class were averaged for comparison to the final approximations of T_a, T_b, T_c, and T_d from equation (3).

The UAV was then hovered above the targeted tree canopy, typically at an altitude of 50 – 75 feet for about ten minutes. The IR sensor allowed for temperature measurements to be taken about every one-tenth of a second, while images were captured about every four seconds. The temperature and GPS data were written to a micro-SD card, and the images were written to a flash card.

RESULTS & DISCUSSION

Image classification

Combinations of the NIR, red, and green bands, along with several vegetative indices derived from these bands, were explored as inputs for the supervised classification. Classification using the NIR and red bands, illustrated in Fig. 3, classified about 96% of pixels correctly, while use of the green and red bands classified about 94% of pixels correctly. Most of the incorrect classifications occurred in distinguishing shaded soil from shaded leaves, an example of which can be seen at the lower end of the vegetation boundary in Fig. 3. There is not much separation between the two classes, so the boundary between them can be somewhat unclear. The slight advantage to using the NIR band did not justify its use, however, when considering the added cost of equipment using a multispectral camera compared to a RGB camera. As a result, this study used the red and green bands for classification.

Evaluation of weighted sum approximation

The applicability of equation (1) was tested by trying to predict T_{meas} based on ground temperature measurements taken by the HHSS. Using the A terms from the classification of each image and the ground temperatures, the predicted temperature, T_{calc}, was calculated using equation (4),

$$T_{calc} = \frac{T_{ma}A_a + T_{mb}A_b + T_{mc}A_c + T_{md}A_d}{A_a + A_b + A_c + A_d} \qquad (4)$$

where T_{ma}, T_{mb}, T_{mc}, and T_{md} represent the average temperature of each class sampled on the ground.

This calculated temperature, T_{calc} was then compared to the temperature from the IR sensor mounted on the UAV corresponding to that image, T_{meas}. If the weighted sum approach was valid, we should be able to predict T_{meas} in this manner. The results of this validation are shown in Fig. 4. Each data point in Fig. 4 represents a single image/temperature record. The linear fit had an r^2 value of 0.96.
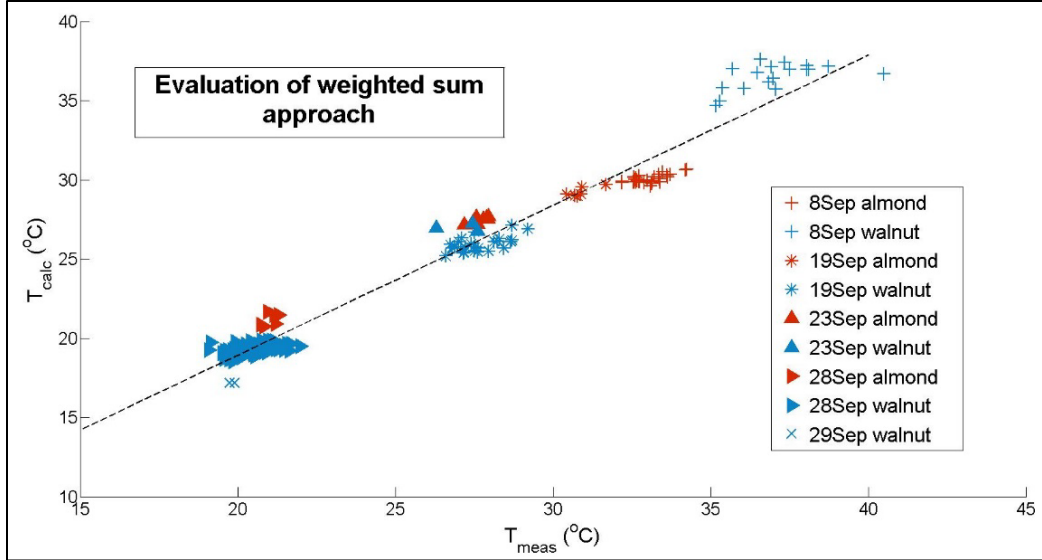
Fig. 4. To test the weighted sum theory, T_{calc} attempted to predict T_{meas} based solely on the classification results and the ground sampled temperatures, as described in equation (4).

Only records classified as at least 95% vegetation were included in the analysis. This eliminated records not applicable to the analysis, such as those obtained during transit to and from the canopy. It also eliminated a lot of the error carried forward by the classifier's difficulty in distinguishing between shaded leaves and shaded soil by ignoring the records with more than 5% soil in the FOV, and it helped to mitigate the error associated with timing discrepancies between the camera and the IR sensor. The records of at least 95% canopy would be situated closer to the center of the canopy, so a small lateral displacement between a temperature measurement and the image capture would not significantly alter the respective A_i terms from equation (4).

Solving for canopy temperature

Assuming the temperature of each class remained constant during each ten-minute flight, each record taken during a flight could be used to populate one equation in the linear system. With at least four records, the four unknowns, T_a, T_b, T_c, and T_d could be approximated as described in equation (3). Fig. 5 illustrates the resulting T_a and T_b, which represented the sunlit leaves and shaded leaves, respectively. The '29Sep walnut' and '23Sep walnut' trials did not have enough records to establish a set of equations, therefore did not carry over to Fig. 5.

For the three almond trials, the approximated values of T_a and T_b differed from their ground truths by 3.6 and 3.1°C, 2.7 and 1.8°C, and 0.4 and 1.6°C, respectively. The respective differences for the four walnut trials were 0.5 and 1.4°C, 1.5 and 1.2°C, 0.5 and 1.9°C, and 1.3 and 0.8°C. The average difference for all walnut temperatures was 1.1°C, compared to 2.2°C for almonds.

Across a range of temperatures from about 16°C to 40°C, the QR decomposition method approximated the temperatures within a reasonably narrow range, resulting in a linear fit with an r^2 value of 0.97.
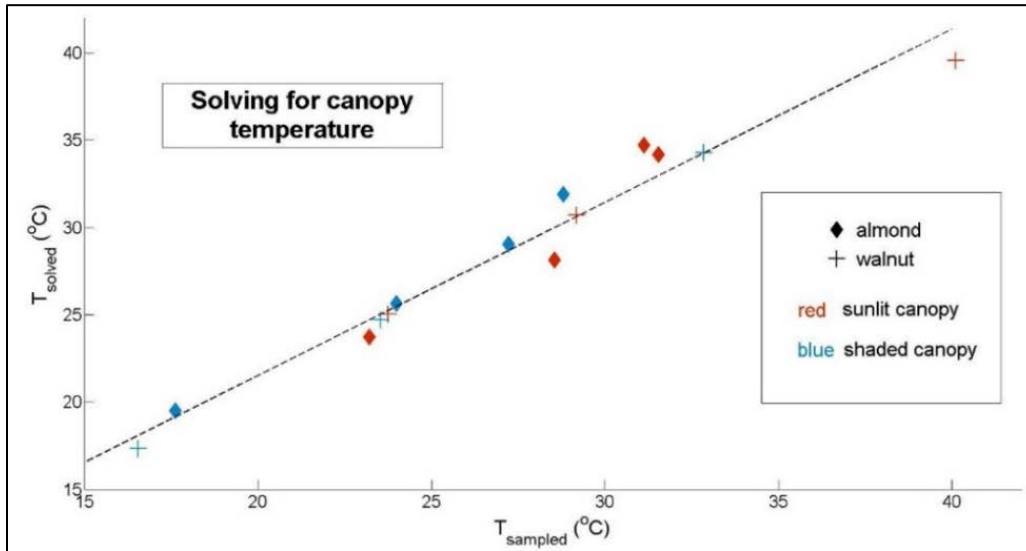

Fig. 5. QR decomposition of each set of linear equations approximated sunlit canopy (T_a) and shaded canopy (T_b).

The better results in walnuts may be a result of the difference in the canopy structure between walnuts and almonds. The walnut canopies were both larger in diameter and composed of much larger leaves. This led to more complete canopy coverage in the FOV than was typically present in almonds, where the soil below the canopy sometimes showed through. As a result, there would be more pixel ambiguity in almonds since more pixels would be expected to be composed partly of soil and partly of vegetation, which would skew the A_i terms in equation (1).

Conclusions

Based on the nine flights used in the analysis, we concluded that an inexpensive IR point sensor can be reliably used to measure T_{can} using a small UAV platform. A properly-timed RGB camera aligned coaxially with the IR sensor can be used to both indicate where the sensor is reading temperature and determine the contents of the temperature measurement. With enough image/temperature records of the same target, a linear approximation technique like QR decomposition shows promising ability to approximate the temperatures of the sunlit and shaded portions of the canopy.

Acknowledgements

REFERENCES

Anderson, M. C., R. G. Allen, A. Morse, and W. P. Kustas. 2012. Use of Landsat thermal imagery in monitoring evapotranspiration and managing water resources. *Remote Sensing of Environment* 122:50-65.

Baluja, J., M. P. Diago, P. Balda, R. Zorer, F. Meggio, F. Morales, and J. Tardaguila. 2012. Assessment of vineyard water status variability by thermal and multispectral imagery using an unmanned aerial vehicle (UAV). *Irrigation Science* 30:511-522.

Carruthers, I., M. W. Rosegrant, and D. Seckler. 1997. Irrigation and food security in the 21st century. *Irrigation and Drainage Systems* 11:83-101.

Chaves, M. M., O. Zarrouk, R. Francisco, J. M. Costa, T. Santos, A. P. Regaldo, M. L. Rodrigues, and C. M. Lopes. 2010. Grapevine under deficit irrigation: hints from physiological and molecular data. *Annals of Botany* 105:661-676.

Cui, N., T. Du, S. Kang, F. Li, J. Zhang, M. Wang, and Z. Li. 2008. Regulated deficit irrigation improved fruit quality and water use efficiency of pear-jujube trees. *Agricultural Water Management* 95(4):489-497.

Fereres, E., and M. A. Soriano. 2007. Deficit irrigation for reducing agricultural water use. *Journal of Experimental Botany* 58(2):147-159.

Garnier, E., and A. Berger. 1985. Testing water potential in peach trees as an indicator of water stress. *Journal of Horticultural Science* 60(1):47-56.

Goldhamer, D. A. 1999. RDI for California canning olives. *Acta Horticulturae* 474:369-372.

Gonzalez-Dugo, V., P. Zarco-Tejada, E. Nicolás, P. A. Nortes, J. J. Alarcón, D. S. Intrigliolo, and E. Fereres. 2013. Using high resolution UAV thermal imagery to assess the variability in the water status of five fruit tree species within a commercial orchard. *Precision Agriculture* 14:660-678.

Intrigliolo, D. S., and J. R. Castel. 2010. Response of plum trees to deficit irrigation under two crop levels: tree growth, yield and fruit quality. *Irrigation Science* 28:525-534.

Jensen, H. E., H. Svendsen, S. E. Jensen, and V. O. Mogensen. 1990. Canopy-air temperature of crops grown under different irrigation regimes in a temperate humid climate. *Irrigation Science* 11:181-188.

Kijne, J. W., R. Barker, and D. J. Molden. 2003. Water productivity in agriculture: limits and opportunities for improvement.

McCutchan, H., and K. A. Shackel. 1992. Stem-water potential as a sensitive indicator of water stress in prune trees. *Journal of American Society of Horticultural Sciences* 117(4):607-611.

Moran, M. S., Y. Inoue, and E. M. Barnes. 1997. Opportunites and limitations for image-based remote sensing in precision crop management. *Remote Sensing of Environment* 61:319-346.

Mulla, D. J. 2013. Twenty five years of remote sensing in precision agriculture: key advances and remaining knowledge gaps. *Biosystems Engineering* 114:358-371.

Naor, A. 1998. Relations between leaf and stem water potentials and stomatal conductance in three field-grown woody species. *Journal of Horticultural Science and Biotechnology* 73(4):431-436.

Scholander, P. F., H. T. Hammel, E. D. Bradstreet, and E. A. Hemmingsen. 1965. Sap pressure in vascular plants. *Science* 148:339-346.

Seelan, S. K., S. Laguette, G. M. Casady, and G. A. Seielstad. 2003. Remote sensing applications for precision agriculture: a learning community approach. *Remote Sensing of Environment* 88:157-169.

Shackel, K. A. 2011. A plant-based approach to deficit irrigation in trees and vines. *Journal of Horticultural Science* 46(2):173-177.

Udompetaikul, V. 2012. Development of a sensor suite for plant water status determination for irrigation management in specialty crops. Dissertation. University of California, Davis, Biological Systems Engineering, Davis, CA

Xiang, H., and L. Tian. 2011. Development of a low-cost agricultural remote sensing system based on an autonomous unmanned aerial vehicle (UAV). *Biosystems Engineering* 108:174-190.